Journal of Materials Chemistry C

PAPER

View Article Online
View Journal | View Issue

Cite this: J. Mater. Chem. C, 2014, 2, 2842

Electrically programmable digital memory behaviors based on novel functional aromatic polyimide/TiO_2 hybrids with a high ON/OFF ratio†

Chih-Jung Chen,‡ Chia-Liang Tsai‡ and Guey-Sheng Liou*

Received 29th December 2013
Accepted 22nd January 2014

DOI: 10.1039/c3tc32580f

www.rsc.org/MaterialsC

A novel solution-processable sulfur-containing poly(*o*-hydroxy-imide) **3SOH-6FPI** with pendant hydroxyl groups and the corresponding polyimide **3SOH-6FPI**/TiO_2 hybrids were synthesized from diamine 4,4′-bis(4-amino-3-hydroxyphenylthio)diphenylsulfide (**3SOH-DA**) and 4,4′-(hexafluoroisopropylidene)-diphthalic anhydride (**6FDA**), and used for memory applications. To enhance the memory behavior, different amounts of TiO_2 were introduced into **3SOH-6FPI** and the corresponding tunable memory properties were investigated. The hydroxyl groups on the backbone of **3SOH-6FPI** could provide reaction sites for organic–inorganic bonding and the homogeneous hybrid thin films could therefore be obtained by controlling the mole ratio of titanium butoxide/hydroxyl groups *via* sol–gel reaction. The resulting hybrid films having different TiO_2 concentrations from 0 wt% to 50 wt% exhibited electrically programmable digital memory properties from DRAM, SRAM, to WORM with a high ON/OFF current ratio (10^8). Furthermore, from the results of the current–voltage *I*–*V* characteristics, the crystalline phase of titania reveals higher trapping ability to increase the retention time in the ON state. In order to get more insight into the switching mechanism of **3SOH-6FPI**/TiO_2 hybrid memory devices, molecular simulation and electrode effects were also discussed in this study.

Introduction

Over the years, the use of polymeric materials in optoelectronic devices has attracted significant attention, such as light-emitting diodes,[1] transistors,[2] solar cells,[3] and electrochromic devices[4] resulting from the advantages of rich structural flexibility, low-cost, solution processability, and three-dimensional stacking capability.[5] Beside these applications, polymeric memory devices[6] have been investigated as a promising alternative to the conventional semiconductor-based memory devices since the first polymer electronic memory reported by Sliva *et al.*[6g] in 1970. As compared to the traditional inorganic memory materials, polymeric memory materials store information in the form of high (ON) and low (OFF) current states and have the superiority of higher data storage density, longer data retention time, fast speed, and low power consumption.[7] Thus, polymeric materials with electrical bistability resulting from conductivity difference in response to the applied electric field begin to stand out conspicuously and have predominance to face the problems and challenges in scaling down from micro-scale to nano-scale.

Although there are numerous kinds of polymers used in memory devices, they are generally classified into four categories as conjugated polymers,[8] polymers with pendent electroactive chromophores,[9] functional polyimides,[10] and hybrid composites.[11] Among these polymers, aromatic polyimides are promising candidates for memory device applications due to the excellent thermal dimensional stability, chemical resistance, mechanical strength, and high ON/OFF current ratio, resulting from the low conductivity in the OFF state. Even though aromatic polyimides have superior properties, they are generally restricted by limited solubility in most organic solvents and their high glass transition (T_g) or melting temperatures caused by the high rigidity of these polymer backbones. For this reason, non-coplanar triphenylamine (TPA) with different substituted groups was introduced into polyimides to enhance the solution processability and act as a donor to facilitate the charge transfer (CT) behavior of polyimides which revealed diverse memory properties.[12] In addition to TPA-based polyimides, the electron-rich sulfur-containing polyimides generally could be easily oxidized and serve as good candidates as electron donors, and also result in high dipole moments, thus leading to stable high-performance memory devices. However, there were only a few organosoluble sulfur-containing polyimides for memory applications.[10i]

Functional Polymeric Materials Laboratory, Institute of Polymer Science and Engineering, National Taiwan University, 1 Roosevelt Road, 4th Sec., Taipei 10617, Taiwan. E-mail: gsliou@ntu.edu.tw

† Electronic supplementary information (ESI) available: Figures: IR spectra, ^{1}H NMR spectrum, UV-visible absorption spectrum, cyclic voltammetric diagram of polyimide **3SOH-6FPI**, TGA and TMA thermograms of **3SOH-6FPI** hybrid materials, and current–voltage (*I*–*V*) characteristics of **ITO/3STP-5/Al** and **ITO/3STP-50/Al** memory devices. Tables: inherent viscosities, GPC data, and solubility of **3SOH-6FPI**. See DOI: 10.1039/c3tc32580f

‡ These authors contributed equally to this work.

Recently, the hybrid composites were extensively prepared for memory device applications and exhibited interesting memory behavior. CT complex formation could be further enhanced by introduction of supplementary components such as organic molecules or metallic particles into the polymer hybrid as electron donors or electron acceptors.[13] As compared with the polymer memory devices with organic molecules or metallic particles, relatively few studies have been conducted on the polymer memory devices containing semiconducting particles.[14] Because of the low LUMO energy level (4.2 eV),[15] TiO_2 could be used as an electron acceptor in the hybrid system to facilitate and stabilize CT complex formation for increasing the retention time of memory characteristics in device applications. Compared with conducting supplementary components such as PCBM, CNT, graphene, and metallic particles,[16] the introduction of TiO_2 could prevent the detriment of decreasing ON/OFF ratios at high TiO_2 content, resulting from the low conductivity in the OFF state.[17]

In this study, we therefore synthesized a new functional polyimide **3SOH-6FPI** from electron-donating 4,4′-bis(4-amino-3-hydroxyphenylthio)diphenylsulfide (**3SOH-DA**) and electron-accepting 4,4′-(hexafluoroisopropylidene)diphthalic anhydride (**6FDA**). Beside higher donor capability, electron-rich sulfur-containing **3SOH-6FPI** was also expected to have high dipole moments and lead to stable high-performance memory devices. **3SOH-6FPI** with different TiO_2 concentrations was prepared and investigated systematically. In order to get more insight into the switching mechanism of **3SOH-6FPI**/TiO_2 memory devices, molecular simulation and electrode effects were also included and discussed in this study.

Results and discussion

Polymer synthesis and basic properties

New **3SOH-6FPI** was synthesized by a one-step method starting from the hydroxyl-containing diamine monomer **3SOH-DA** and aromatic tetracarboxylic dianhydrides **6FDA** in the presence of a catalytic amount of isoquinoline at 170–180 °C as shown in Scheme 1. The formation of **3SOH-6FPI** was confirmed by FTIR and NMR measurements. The IR spectrum of **3SOH-6FPI** (film) exhibited broad absorption bands in the region of 2500 to 3700 cm^{-1} (O–H stretch) and characteristic imide absorption bands at 1785 (asymmetrical C=O), 1722 (symmetrical C=O), 1390 (C–N), 1105 (Ar–S–Ar), 1256 (C–F), and 748 cm^{-1} (imide ring deformation) as shown in Fig. S1.† Furthermore, the IR spectrum of 50 wt% **3SOH-6FPI**/TiO_2 hybrids (**3STP-50**) revealed additional absorption bands at 650 to 800 cm^{-1} (Ti–O–Ti). The ^1H NMR result of **3SOH-6FPI** is also shown in Fig. S2† (DMSO-d_6, δ, ppm): 6.80 (m, 4H), 7.33 (m, 10H), 7.71 (s, 2H), 7.91 (d, 2H), 8.10 (d, 2H) and 10.08 (s, 2H, OH). The inherent viscosity, weight-average molecular weight (M_w), and polydispersity index (PDI) of the obtained polyimide are shown in Table S1.† The solubility behavior of **3SOH-6FPI** was investigated and the results are summarized in Table S2.† **3SOH-6FPI** revealed high solubility in common organic solvents for the solution process in memory device applications. The thermal properties of the **3SOH-6FPI** and **3SOH-6FPI**/TiO_2 hybrid materials are also summarized in Table 1. Typical TGA and TMA curves of **3SOH-6FPI** and hybrids are depicted in Fig. S3 and S4,† respectively. These hybrid materials both in nitrogen and air exhibited excellent thermal stability and higher carbonized residue (char yield) with increasing TiO_2 content. The titania contents in the hybrid materials could be estimated based on the char yields under air flow, which were in good agreement with the theoretical content and ensured successful incorporation of the nanocrystalline-titania. Meanwhile, the coefficient of thermal expansion (CTE) is one of the important designing parameters for the application of polymer films in the microelectronic field, and the CTE values of **3SOH-6FPI** and **3SOH-6FPI**/TiO_2 hybrid films were measured and summarized in Table 1. **3STP-50** exhibited the highest T_g and the lowest CTE among these hybrid materials.

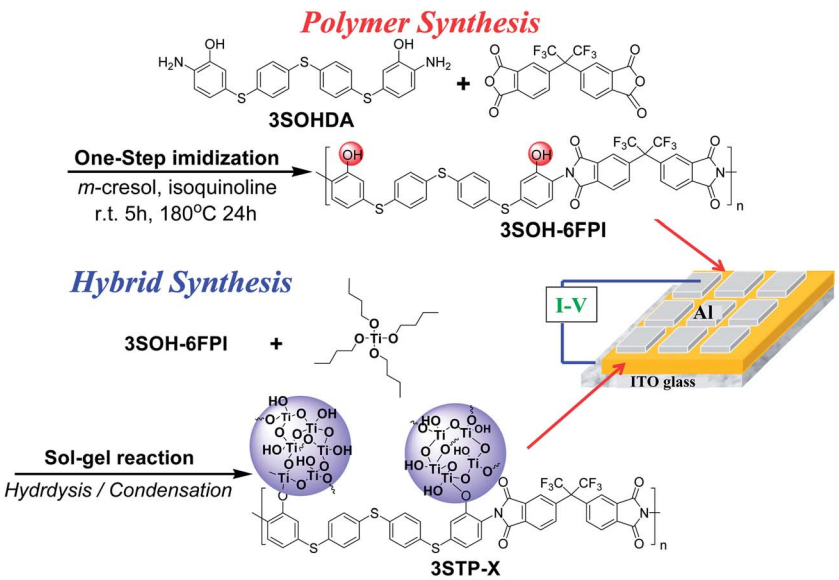

Scheme 1 Synthesis of 3SOH-6FPI, hybrid materials, and a schematic diagram of the memory device.

Absorption and electrochemistry

The UV-vis absorption spectrum of **3SOH-6FPI** is depicted in Fig. S5† and the onset wavelength of optical absorption was utilized to obtain the optical energy band gap (E_g) of the polyimide. The electrochemical behavior of **3SOH-6FPI** was investigated by cyclic voltammetry (CV) conducted by using cast films on an indium–tin oxide (ITO)-coated glass slide as a working electrode in anhydrous acetonitrile (CH_3CN), using 0.1 M of tetrabutylammonium perchlorate (TBAP) as a supporting electrolyte. The typical CV diagram of **3SOH-6FPI** is shown in Fig. S6.† The redox potentials of the polyimide as well as its respective highest occupied molecular orbital (HOMO) and lowest unoccupied molecular orbital (LUMO) (*versus* vacuum) were calculated and are summarized in Table 2. The onset oxidation of **3SOH-6FPI** exhibited at 1.11 V. The HOMO levels or ionization potentials (*versus* vacuum) of **3SOH-6FPI** could be estimated from the onset of its oxidation in CV experiments as 5.55 eV (on the basis that ferrocene/ferrocenium is 4.8 eV below the vacuum level with $E_{onset} = 0.36$ V).

Memory device characteristics

The memory behavior of **3SOH-6FPI** and **3SOH-6FPI**/TiO_2 hybrids was depicted by the current–voltage (*I–V*) characteristics of an ITO/polymer/Al sandwich device as shown in Scheme 1. Within the sandwich device, a polymer or hybrid film was used as an active layer between Al and ITO as the top and bottom electrodes. To exclude the effect of the polymer film thickness on memory properties, a standard thickness (50 nm) was used without specific mention. Fig. 1(a) shows the *I–V* result of **3SOH-6FPI**, which was measured with a compliance current of 0.01 A. During the first positive sweep from 0 V to 6 V, the device stayed in the low-conductivity (OFF) state with a current range of 10^{-12} to 10^{-13} A, which means that the positive applied voltage could not switch the memory device on. In contrast, the current increased abruptly from 10^{-12} to 10^{-13} to 10^{-5} A (high-conductivity state) at a threshold voltage of −4.9 V in the second negative sweep, indicating the transition from the OFF state to the high-conductivity (ON) state. In a memory device, this OFF-to-ON transition can be defined as a "writing" process. The device remained in the ON state during the subsequent negative scan (the third sweep) and then the positive scan (the fourth sweep). The memory device could not be reset to the initial OFF state by the application of a reverse scan implying the non-erasable behavior. The fifth sweep was conducted after turning off the power for about 35 seconds, and found that the ON state had relaxed to the steady OFF state. It suggests that the ON state could be retained for a short period of time after the removal of applied voltage and then relaxed to the initial OFF state eventually. The device could also be reprogrammed by starting from the OFF state to the ON state again with a threshold voltage of −4.7 V in the fifth sweep, and kept in the ON state in the subsequent sixth sweep. The fifth and sixth sweeps were conducted to confirm that the memory device is rewritable. The short retention time of the ON state indicates that the memory device of **3SOH-6FPI** showed volatile dynamic random access memory (DRAM) properties. To make a comparison with **3SOH-6FPI**, a structurally similar polyimide **3S-6FPI** without hydroxyl groups was also prepared, and the *I–V* result of **3S-6FPI** revealed almost the same DRAM behavior as **3SOH-6FPI** shown in

Table 1 Thermal and optical properties of 3SOH-6FPI hybrid films

	Thermal properties							
			T_d^{5c} (°C)		T_d^{10c} (°C)			
Index	T_g[a] (°C)	CTE[b] (ppm K^{-1})	N_2	Air	N_2	Air	R_{w800}[d] (%)	R_{w800}[e] (%)
3SOH-6FPI	230	72	350	465	475	490	59	0
3STP-5	268	68	490	480	530	530	64	4.7
3STP-10	278	60	500	495	565	560	70	9.7
3STP-30	289	53	525	505	595	575	74	29.3
3STP-50	315	41	540	535	605	580	82	49.2

[a] Glass transition temperature measured by TMA with a constant applied load of 50 mN at a heating rate of 10 °C min^{-1} by tension mode. [b] The CTE data were determined over a 50–200 °C range by expansion mode. [c] Temperature at which 5% and 10% weight loss occurred, respectively, recorded by TGA at a heating rate of 20 °C min^{-1} and a gas flow rate of 30 cm^3 min^{-1}. [d] Residual weight percentages at 800 °C under nitrogen flow. [e] Residual weight percentages at 800 °C under air flow.

Table 2 Electrochemical and optical properties of 3SOH-6FPI

	UV-vis absorption (nm)		Oxidation potential (V) (*vs.* Ag/AgCl in CH_3CN)			
Polymer	λ_{max}	λ_{onset}	E_{onset}	E_g[a] (eV)	HOMO[b] (eV)	LUMO (eV)
3SOH-6FPI	299	349	1.11	3.54	5.55	2.01

[a] The data were calculated from polymer films by the equation: $E_g = 1240/\lambda_{onset}$ (energy gap between HOMO and LUMO). [b] The HOMO energy levels were calculated from CV and were referenced to ferrocene (4.8 eV; onset = 0.36 V).

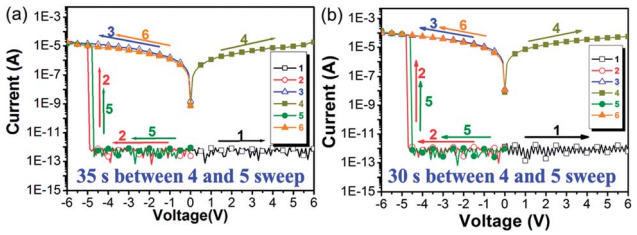

Fig. 1 Current–voltage (*I–V*) characteristics of the ITO/polyimide/Al memory devices: (a) **3SOH-6FPI** and (b) **3S-6FPI**.

Fig. 1(b), indicating that these two hydroxyl groups in each repeating unit of **3SOH-6FPI** have no trap effect on the behavior of memory properties. Furthermore, the *I–V* result of **3S-6FPI** is quite different from the behavior published before maybe due to a different film thickness and operating system.[10i]

Fig. 2(a) depicts the *I–V* result of **3STP-7**. A sharp increase of the current could be observed at −4.5 V during the second negative sweep. The device of **3STP-7** maintained in the ON state after turning off the power for a longer period of time than **3SOH-6FPI**. The fifth sweep was conducted after turning off the power for about 7 minutes and the device could be switched to the ON state again at a threshold voltage of −4.2 V. The longer retention time in the ON state yet volatile, as well as the randomly accessible ON and OFF states is similar to the data remanence behavior of static random access memory (SRAM). Fig. 2(b)–(d) revealed the memory results of polyimide hybrids **3STP-10** and **3STP-30**, respectively. Compared to volatile DRAM and SRAM properties, the ON state of **3STP-10** and **3STP-30** could be kept even after turning off the power for 30 minutes or longer time since it has been switched on. Thus, this *I–V* characteristic indicates that the memory devices based on **3STP-10** and **3STP-30** hybrid films exhibited non-volatile write-once-read-many-times memory (WORM) properties. Furthermore, the higher TiO_2 containing the hybrid film **3STP-30** could be switched to the ON state by a positive voltage of 2.9 V as shown in Fig. 2(d). In order to explore the transition from DRAM to SRAM (7 minutes) by introducing 7 wt% TiO_2 into **3SOH-6FPI**, the intermediate **3STP-5** hybrid films were prepared to fabricate the sandwich device for investigating the electrical characteristics. DRAM and SRAM properties were both present in the device of **3STP-5** as shown in Fig. S7.† The probability of the resulting DRAM and SRAM behaviors of **3STP-5** was 50% for DRAM and 50% for SRAM, while the SRAM behavior of **3STP-5** only possessed 2 minute retention time. The memory properties of **3STP-50** were also investigated and are available in the ESI.† The memory properties of **3SOH-6FPI** hybrid materials with different TiO_2 contents from 0 wt% to 50 wt% are summarized in Fig. 3. Generally, the memory device reveals longer retention time and could be switched to the ON state by applying both positive and negative voltages with increasing the content of TiO_2.

In addition, the polyimide–TiO_2 hybrid film with amorphous TiO_2 (a-TiO_2) **3STP-a*X***, which was only heated at 150 °C to remove the solvent, and the memory behavior were depicted by the current–voltage (*I–V*) characteristics as shown in Fig. 4. Fig. 4(a) and (b) summarize the memory results of polyimide hybrids **3STP-a7** and **3STP-a10**, which have longer retention time in the ON state yet volatile, as well as the randomly accessible ON and OFF states similar to the data remanence behavior of SRAM (2 min) and SRAM (5 min) respectively. The ON state of **3STP-a30** (Fig. 4(c) and (d)) could be kept even after turning off power for 30 minutes or longer time since it has been switched on. Thus, this *I–V* characteristic indicates that the memory device based on **3STP-a30** hybrid films revealed non-volatile WORM memory properties. To make a comparison with **3STP-*X***, the difference is only the crystalline form of TiO_2. The *I–V* characteristics indicates that the memory devices based

PI+TiO_2 hybrid	0wt%	5wt%	7wt%	10wt%	30wt%	50wt%
memory property	DRAM (35sec)	50% DRAM/ 50% SRAM (2min)	SRAM (7min)	WORM	WORM (biswitch)	WORM (biswitch)

Amounts of acceptor increase

Fig. 3 Memory properties of **3SOH-6FPI** hybrid materials.

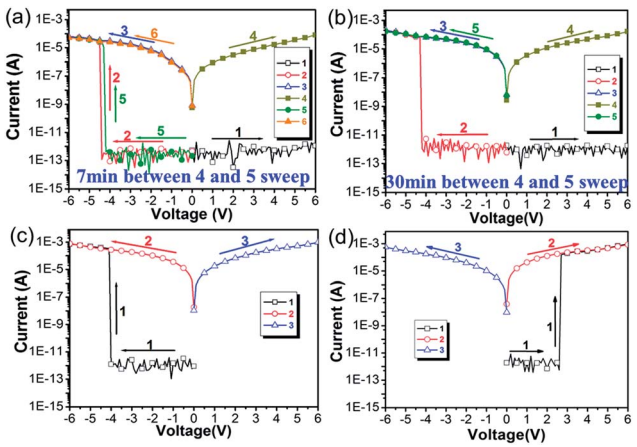

Fig. 2 Current–voltage (*I–V*) characteristics of the ITO/hybrid material/Al memory devices: (a) **3STP-7**, (b) **3STP-10**, and (c and d) **3STP-30**.

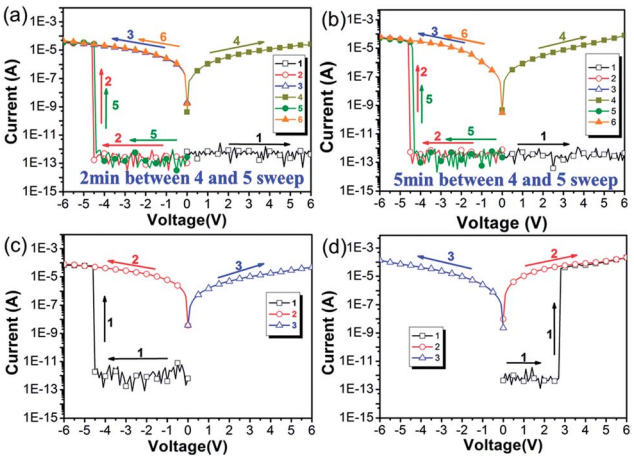

Fig. 4 Current–voltage (*I–V*) characteristics of the ITO/hybrid material (with a-TiO_2)/Al memory devices (a) **3STP-a7**, (b) **3STP-a10**, and (c and d) **3STP-a30**.

on **3STP-a*X*** have shorter retention time in the ON state compared to the devices based on **3STP-*X***. Because the a-TiO_2 had larger disorder and higher concentration of imperfections such as impurities, dangling bonds, and microvoids that typically lead to unwanted electronic states resulting in the reduction of charge migration and a rapid recombination of electron–hole pairs.[18]

Furthermore, the XRD patterns of the hybrid films heated to 150 and 350 °C are depicted in Fig. 5(a) and (b), respectively, revealing that titania only heated to 150 °C in the PI hybrid films was amorphous. The intensity of a titania crystalline peak gradually increased in the range $2\theta = 23–27°$ with increasing titania content when annealed at 350 °C. The enhanced titania crystallization could be obviously observed in the case of **3STP-50** with four peaks, 25.5°, 38.4°, 48.3°, and 54.8°, corresponding to the (101), (112), (200), and (211) crystalline planes of the anatase titania phase, respectively.[19] From the result of XRD patterns, the TiO_2 crystalline phase of PI hybrids could be transformed from amorphous into crystalline phase by annealing at 350 °C.[20]

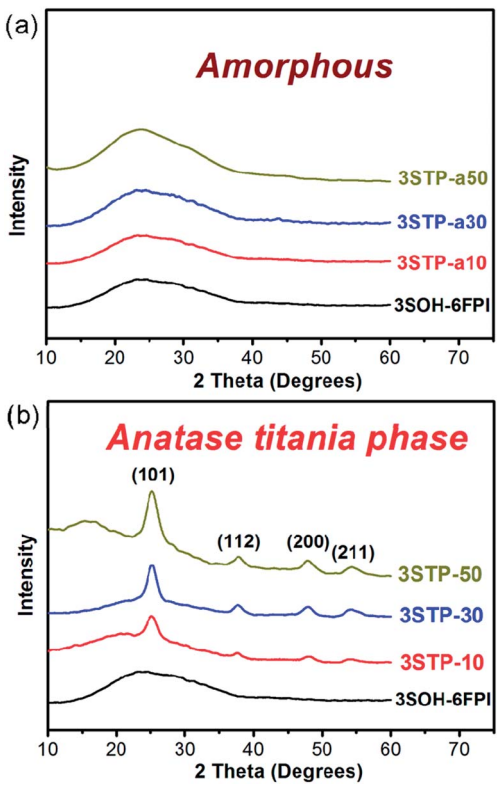

Fig. 5 XRD patterns of 3SOH-6FPI and hybrid materials heated to (a) 150 °C and (b) 350 °C.

Switching mechanism

In order to get more insight into the memory behavior of polyimide **3SOH-6FPI**, molecular simulation on the basic unit was carried out by DFT/B3LYP/6-31G(d) with the Gaussian 09 program as shown in Fig. 6. According to the simulation results, **3SOH-6FPI** has a high dipole moment (3.60 D), and the high

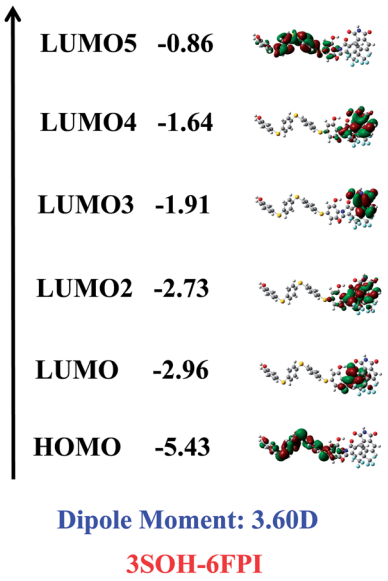

Fig. 6 Calculated molecular orbitals and corresponding energy levels of the basic units (BUs) for 3SOH-6FPI.

dipole moment facilitates the CT complex of **3SOH-6FPI** and its corresponding hybrid materials for increasing the retention time of memory devices after turning off the applied power. Furthermore, the HOMO of **3SOH-6FPI** is located mainly at the electron-donating sulfur-containing diamine moiety, while LUMOs are distributed around electron-withdrawing phthalimide units, adjacent phenyl ring, and hexafluoroisopropylidene group. According to previous literature,[6a] when the applied electric field reaches the switching-on voltage, some electrons at the HOMO accumulate energy and transit to the LUMO to form a CT complex (ON state) by different ways. When the intra- or intermolecular CT occurred by the applied electric field, the generating holes can be delocalized to the sulfur-containing diamine moieties forming an open channel in the HOMO of polyimides for the charge carriers (holes) to migrate through.

Based on this proposed mechanism, when the negative sweep was conducted, the hole could be injected from the bottom electrode ITO to the HOMO of the polymer due to the lower band gap between ITO (−4.8 eV) and HOMO of the polymer as shown in Fig. 7. In contrast, during positive sweep, the hole is hard to be injected from the top electrode Al into the HOMO of the polymer because of the larger energy gap between the work function of Al (−4.2 eV) and the HOMO of the polymer, thus the memory device could not be switched to the ON state. However, with the introduction of TiO_2 into **3SOH-6FPI**, the hybrid materials therefore have a lower LUMO energy level and could be switched to the ON state at positive sweep. This phenomenon could be attributed to the smaller band gap between LUMO of TiO_2 (−4.2 eV) and work function of Al (−4.2 eV) and ITO (−4.8 V). In addition to switching-on voltage, introduction of TiO_2 as electron acceptors into **3SOH-6FPI** could also stable the charge transfer complex and thus **3SOH-6FPI**/TiO_2 hybrid materials with higher TiO_2 contents revealed longer retention time. In order to understand the switching mechanism further, the **3SOH-6FPI** and **3STP-30** memory devices with

the configuration ITO/polymer/Au were prepared and the memory properties were investigated as shown in Fig. 8 and 9, respectively. The Au electrode with a work function of −5.1 eV is advantageous for the switching-on of **3SOH-6FPI** and **3STP-30** memory devices in positive sweep as shown in Fig. 10.

TEM was also used to characterize the morphology of the prepared hybrid films as shown in Fig. 11. The dark regions indicate the formation of TiO_2 clusters with domain size around 3–5 nm which were well dispersed in the matrix **3SOH-6FPI** even at 50 wt% TiO_2 content. Compared to previous literature,[21] hybrid films with much enhanced nano-scale distribution of

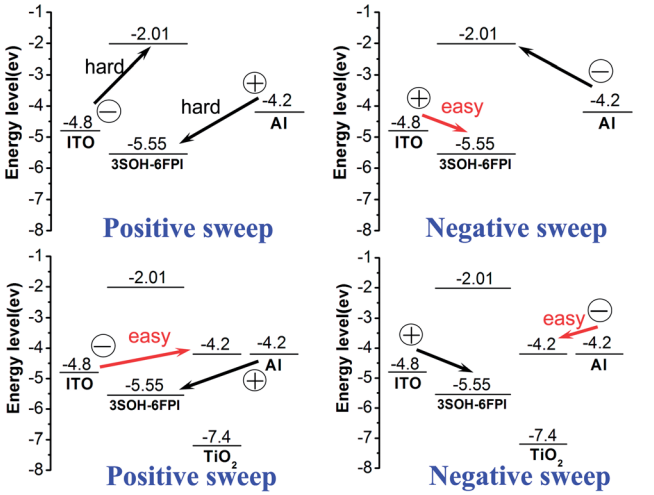

Fig. 7 HOMO and LUMO energy levels of **3SOH-6FPI** and TiO_2 along with the work function of the electrodes.

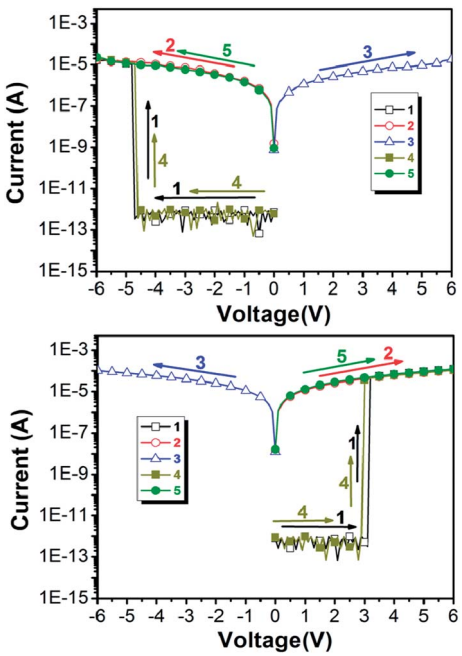

Fig. 8 Current–voltage (*I*–*V*) characteristics of the ITO/**3SOH-6FPI**/Au memory device. (The fourth sweep was conducted about 35 seconds after turning off the power.)

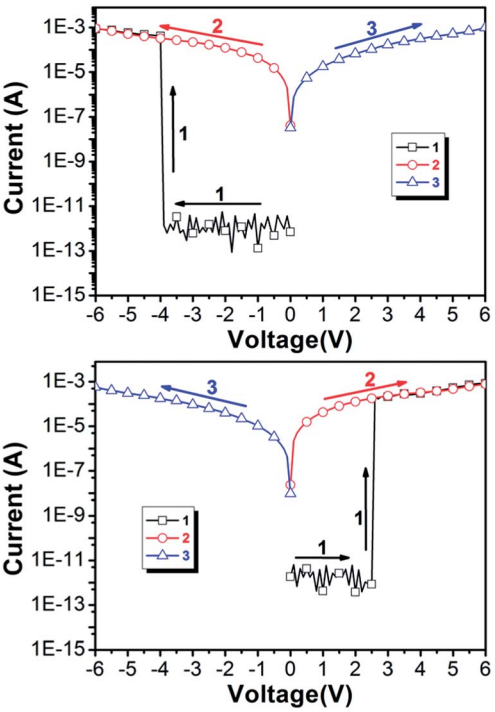

Fig. 9 Current–voltage (*I*–*V*) characteristics of the ITO/**3STP-30**/Au memory device.

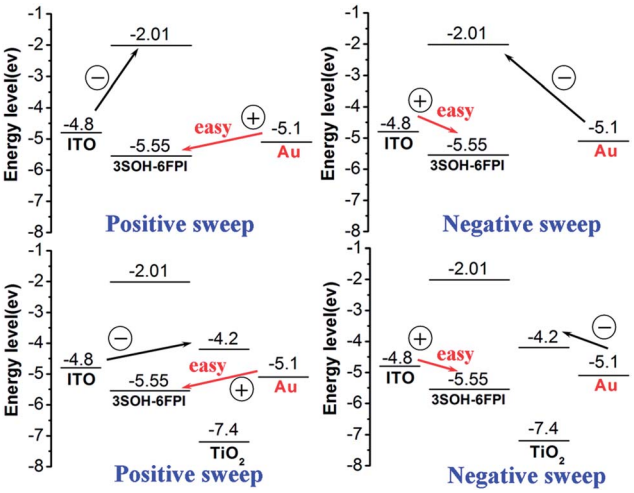

Fig. 10 HOMO and LUMO energy levels of **3SOH-6FPI** and TiO_2 along with the work function of the electrodes.

TiO_2 in this study could afford excellent film quality and avoid filament formation. Besides, the obtained PI hybrids with a higher amount of TiO_2 and very small domain size within the matrix **3SOH-6FPI** could facilitate and stabilize the charge separation state, hindering from back recombination even under the reverse bias. Thus, the high conductance state can be retained for much longer time, tuning the devices from DRAM to SRAM, and even WORM type memory characteristics. Furthermore, a high ON/OFF ratio of these hybrid materials could be maintained even at high TiO_2 content due to the

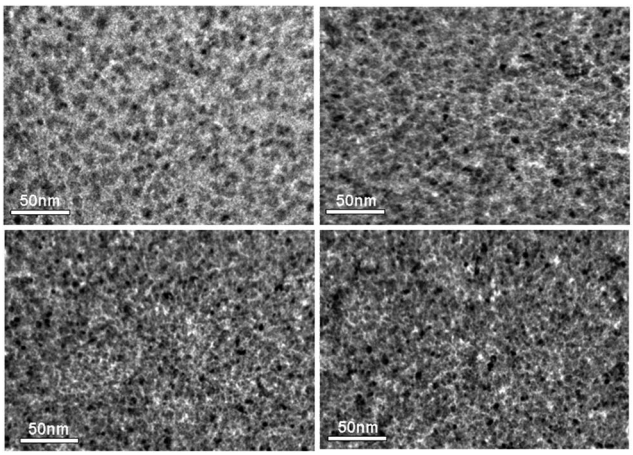

Fig. 11 TEM images of the hybrid materials (a) **3STP-5**, (b) **3STP-10**, (c) **3STP-30** and (d) **3STP-50**.

insulator behavior of TiO_2, resulting in low conductivity in the OFF state.

Conclusions

A novel solution-processable sulfur-containing polyimide **3SOH-6FPI** with pendant hydroxyl groups was synthesized and used for the comparison of memory behavior with the corresponding polyimide without pendant hydroxyl groups. The hydroxyl groups could react with titanium butoxide ($Ti(OBu)_4$), providing organic–inorganic bonding at each repeating unit at different TiO_2 concentrations from 0 wt% to 50 wt%. The results indicated that hybrid films have a very small domain size of TiO_2 of around 3–5 nm and tunable memory properties from DRAM, SRAM, to WORM with a high ON/OFF current ratio (10^8). Furthermore, the effect of crystalline phase of TiO_2 in the PI hybrid films on the memory behavior was also investigated, and anatase titania exhibited higher trapping ability to increase the retention time in the ON state than amorphous titania of **3SOH-6FPI**/TiO_2.

Experimental section

Materials

4,4′-Bis(4-amino-3-hydroxyphenylthio)diphenyl sulfide (**3SOH-DA**) and 4,4′-thiobis[(*p*-phenylenesulfanyl)aniline] **(3S-DA)** were prepared according to a previously reported procedure.[10i,20c] 2,2-Bis(3,4-dicarboxyphenyl)hexafluoropropane dianhydride (6FDA) (Chriskev) was purified by vacuum sublimation. Tetrabutylammonium perchlorate (TBAP) (Acros) was recrystallized twice with ethyl acetate under a nitrogen atmosphere and then dried *in vacuo* prior to use. **3S-6FPI** was prepared according to previous literature.[10i] All other reagents were used as received from commercial sources.

Polymer synthesis

The stoichiometric mixture of the hydroxyl diamine **3SOH-DA** (0.93 g, 2.00 mmol), the dianhydride **6FDA** (0.89 g, 2.00 mmol), and a few drops of isoquinoline in *m*-cresol (7 mL) was stirred at an ambient temperature under nitrogen. After the solution was stirred for 5 h, it was heated to 170–180 °C and maintained at that temperature for 24 h. During this time, the water of imidization was allowed to distill from the reaction mixture along with *m*-cresol. The *m*-cresol was continually replaced so as to keep the total volume of the solution constant. After the solution was allowed to cool to ambient temperature, the viscous solution then was poured slowly into 300 mL of methanol with stirring. The precipitated polymer was collected by filtration, washed thoroughly with hot methanol, and dried under reduced pressure at 150 °C for 15 h. The inherent viscosity of the obtained polyimide **3SOH-6FPI** was 0.49 dL g^{-1} (measured at a concentration of 0.5 g dL^{-1} in DMAc at 30 °C). The IR spectrum of **3SOH-6FPI** (film) exhibited broad absorption bands in the region of 2500 to 3700 cm^{-1} (O–H stretch) and characteristic imide absorption bands at 1785 (asymmetrical C═O), 1722 (symmetrical C═O), 1390 (C–N), 1105 (Ar–S–Ar), 1256 (C–F), and 748 cm^{-1} (imide ring deformation); yield: 98%. Anal. calcd for $(C_{42}H_{22}N_2O_6S_3)_n$ (872.83)$_n$: C, 59.17%; H, 2.54%; N, 3.21%; S, 11.20%. Found: C, 57.54%; H, 2.91%; N, 3.39%; S, 10.83%.

Preparation of the polyimide–TiO_2 hybrid films

The preparation of the polyimide–TiO_2 hybrid **3STP-50** was used as an example to illustrate the general synthesis route to the hybrids **3STP-*X***. Firstly, 0.05 g (0.057 mmol) of **3SOH-6FPI** was dissolved in 3 mL of DMAc, and 0.05 g of HCl (37 wt%) was added very slowly to the organic solution and stirred at room temperature for 0.5 h. Then, 0.21 mL (0.62 mmol) of $Ti(OBu)_4$ dispersed in 0.21 mL of *n*-butanol was added drop-wise to the above solution with a syringe, and the mixture was stirred at room temperature for further 1 hour. The resulting precursor solution was then filtered through a 0.45 μm PTFE filter before being spin-coated onto an ITO glass plate at 1000–2000 rpm for 60 seconds. The film was treated by the multi-step heating process of 100, 150, 250 °C for 20 min, and 350 °C for 90 min for obtaining PI hybrid films with anatase crystalline titanium oxide (c-TiO_2). While, the resulting film **3STP-a*X*** with amorphous TiO_2 (a-TiO_2) was only treated by the heating process of 100 and 150 °C for 30 min to remove the solvent.

Measurement of basic properties

Fourier transform infrared (FT-IR) spectra were recorded on a PerkinElmer Spectrum 100 Model FT-IR spectrometer with resolution 1 cm^{-1} and number of scans 4. The ^1H NMR spectrum was recorded on a Bruker AC-300 MHz spectrometer in DMSO-d_6, using tetramethylsilane as an internal reference, and peak multiplicity was reported as follows: s, singlet; d, doublet; m, multiplet. The inherent viscosity was determined at 0.5 g dL^{-1} concentration using a Tamson TV-2000 viscometer at 30 °C. Gel permeation chromatographic (GPC) analysis was carried out on a Waters chromatography unit interfaced with a Waters 2410 refractive index detector, calibrating with polystyrene standards. Two Waters 5 μm Styragel HR-2 and HR-4 columns (7.8 mm I. D. × 300 mm) were connected in series with NMP as the eluent at a flow rate of 0.5 mL min^{-1} at 40 °C. Thermogravimetric analysis

(TGA) was conducted with a TA SDT Q600. Experiments were carried out on approximately 6–8 mg samples heated in flowing nitrogen or air (flow rate = 20 cm^3 min^{-1}) at a heating rate of 20 °C min^{-1}. The coefficient of thermal expansion (CTE) and glass transition temperatures (T_g) are measured on a dilatometer (TA instrument TMA Q400EM). The TMA experiments were conducted from 50 to 450 °C at a scan rate of 10 °C min^{-1} with a tensile probe under an applied constant load of 50 mN. T_g was taken as the onset temperature of probe displacement on the TMA traces. The CTE data were determined in the range of 50–200 °C by using a film–fiber probe with expansion mode. Cyclic voltammetry (CV) was performed with a Bioanalytical System Model CV-27 and conducted with the use of a three-electrode cell in which ITO (polymer films area about 0.5 cm × 1.2 cm) was used as the working electrode and a platinum wire as the auxiliary electrode at a scan rate of 100 mV s^{-1} against a Ag/AgCl reference electrode in anhydrous CH_3CN, using 0.1 M of TBAP as the supporting electrolyte. All cell potentials were taken by using a homemade Ag/AgCl, KCl (sat.) reference electrode. The microstructure of the prepared films was examined by using a JOEL JEM-1230 transmission electron microscope (TEM). UV-visible absorption was recorded on a UV-visible spectrophotometer (Hitachi U-4100).

Fabrication and measurement of the memory devices

The memory devices were fabricated with the configuration of ITO/thin film/Al or Au. The ITO glass used for memory devices was precleaned by ultrasonication with water, acetone, and isopropanol each for 15 min. The hybrid thin films were prepared according to the previous procedure using ITO as a substrate. The film thickness was adjusted to be around 50 nm. Finally, a 300 nm thick Al or Au top electrode was thermally evaporated through the shadow mask (recorded device units of 0.5 × 0.5 mm^2 in size) at a pressure of 10^{-7} Torr with a uniform depositing rate of 3–5 Å s^{-1}. The electrical characterization of the memory device was performed using a Keithley 4200-SCS semiconductor parameter analyzer equipped with a Keithely 4205-PG2 arbitrary waveform pulse generator. ITO was used as the cathode (maintained as common), and Al or Au was set as the anode during the voltage sweep. The probe tip used 10 μm diameter tungsten wire attached to a tinned copper shaft with a point radius <0.1 μm (GGB Industries, Inc.).

Molecular simulation

Molecular simulation in this study was carried out with the Gaussian 09 program package. Equilibrium ground state geometry and electronic properties of basic units of these aromatic polyimides were optimized by means of the density functional theory (DFT) method at the B3LYP level of theory (Beckesstyle three-parameter density functional theory using the Lee–Yang–Parr correlation functional) with the 6-31G(d) basic set.

Acknowledgements

We gratefully acknowledge the National Science Council of Taiwan for the financial support.

References and notes

1 (*a*) R. H. Friend, R. W. Gymer, A. B. Holmes, J. H. Burroughes, R. N. Marks, C. Taliani, D. D. C. Bradley, D. A. Dos Santos, J. L. Bredas, M. Logdlund and W. R. Salaneck, *Nature*, 1999, **397**, 121; (*b*) Q. Peng, E. T. Kang, K. G. Neoh, D. Xiaob and D. Zou, *J. Mater. Chem.*, 2006, **16**, 376; (*c*) Y. Shao, X. Gong, A. J. Heeger, M. Liu and A. K. Y. Jen, *Adv. Mater.*, 2009, **21**, 1972.

2 (*a*) H. Yan, Z. H. Chen, Y. Zheng, C. Newman, J. R. Quinn, F. Dotz, M. Kastler and A. Facchetti, *Nature*, 2009, **457**, 679-U1; (*b*) Y. H. Chou, H. J. Yen, C. L. Tsai, W. Y. Lee, G. S. Liou and W. C. Chen, *J. Mater. Chem. C*, 2013, **1**, 3235.

3 (*a*) G. Yu, J. Gao, J. C. Hummelen, F. Wudl and A. J. Heeger, *Science*, 1995, **270**, 1789; (*b*) C. J. Brabec, N. S. Sariciftci and J. C. Hummelen, *Adv. Funct. Mater.*, 2001, **11**, 15; (*c*) M. H. Chen, J. Hou, Z. Hong, G. Yang, S. Sista, L. M. Chen and Y. Yang, *Adv. Mater.*, 2009, **21**, 4238.

4 (*a*) H. J. Yen and G. S. Liou, *Chem. Mater.*, 2009, **21**, 4062; (*b*) H. J. Yen, H. Y. Lin and G. S. Liou, *Chem. Mater.*, 2011, **23**, 1874; (*c*) H. J. Yen and G. S. Liou, *Polym. Chem.*, 2012, **3**, 255; (*d*) S. V. Vasilyeva, P. M. Beaujuge, S. J. Wang, J. E. Babiarz, V. W. Ballarotto and J. R. Reynolds, *ACS Appl. Mater. Interfaces*, 2011, **3**, 1022; (*e*) E. Puodziukynaite, J. L. Oberst, A. L. Dyer and J. R. Reynolds, *J. Am. Chem. Soc.*, 2012, **134**, 968; (*f*) E. P. Knott, M. R. Craig, D. Y. Liu, J. E. Babiarz, A. L. Dyer and J. R. Reynolds, *J. Mater. Chem.*, 2012, **22**, 4953; (*g*) P. M. Beaujuge, S. V. Vasilyeva, D. Y. Liu, S. Ellinger, T. D. McCarley and J. R. Reynolds, *Chem. Mater.*, 2012, **24**, 255.

5 A. Stikeman, *Technol. Rev.*, 2002, 31.

6 (*a*) Q. D. Ling, F. C. Chang, Y. Song, C. X. Zhu, D. J. Liaw, D. S. H. Chan, E. T. Kang and K. G. Neoh, *J. Am. Chem. Soc.*, 2006, **128**, 8732; (*b*) C. J. Chen, H. J. Yen, W. C. Chen and G. S. Liou, *J. Polym. Sci., Part A: Polym. Chem.*, 2011, **49**, 3709; (*c*) Y. Q. Li, Y. Y. Chu, R. C. Fang, S. J. Ding, Y. L. Wang, Y. Z. Shen and A. M. Zheng, *Polymer*, 2012, **53**, 229; (*d*) B. L. Hu, F. Zhuge, X. J. Zhu, S. S. Peng, X. X. Chen, L. Pan, Q. Yan and R. W. Li, *J. Mater. Chem.*, 2012, **22**, 520; (*e*) Y. C. Hu, C. J. Chen, H. J. Yen, K. Y. Lin, J. M. Yeh, W. C. Chen and G. S. Liou, *J. Mater. Chem.*, 2012, **22**, 20394; (*f*) T. Kurosawa, T. Higashihara and M. Ueda, *Polym. Chem.*, 2013, **4**, 16; (*g*) P. O. Sliva, G. Dir and C. Griffiths, *J. Non-Cryst. Solids*, 1970, **2**, 316.

7 (*a*) H. Gruber, *Research Policy*, 2000, **29**, 725; (*b*) S. Moller, C. Perlov, W. Jackson, C. Taussig and S. R. Forrest, *Nature*, 2003, **426**, 166.

8 (*a*) X. D. Zhuang, Y. Chen, G. Liu, P. P. Li, C. X. Zhu, E. T. Kang, K. G. Noeh, B. Zhang, J. H. Zhu and Y. X. Li, *Adv. Mater.*, 2010, **22**, 1731; (*b*) X. D. Zhuang, Y. Chen, B. X. Li, D. G. Ma, B. Zhang and Y. Li, *Chem. Mater.*, 2010, **22**, 4455; (*c*) S. J. Liu, W. P. Lin, M. D. Yi, W. J. Xu, C. Tang, Q. Zhao, S. H. Ye, X. M. Liu and W. Huang, *J. Mater. Chem.*, 2012, **22**, 22964; (*d*) S. Baek, D. Lee, J. Kim, S. H. Hong, O. Kim and M. Ree, *Adv. Funct. Mater.*, 2007, **17**, 2637; (*e*) H. C. Wu, A. D. Yu, W. Y. Lee, C. L. Liu and

W. C. Chen, *Chem. Commun.*, 2012, **48**, 9135; (*f*) F. L. Ye, P. Y. Gu, F. Zhou, H. F. Liu, X. P. Xu, H. Li, Q. F. Xu and J. Lu, *Polymer*, 2013, **54**, 3324; (*g*) D. Wang, H. Li, N. Li, Y. Zhao, Q. Zhou, Q. Xu, J. Lu and L. Wang, *Mater. Chem. Phys.*, 2012, **134**, 273.

9 (*a*) B. Zhang, G. Liu, Y. Chen, C. Wang, K. G. Neoh, T. Bai and E. T. Kang, *ChemPlusChem*, 2012, **77**, 74; (*b*) S. J. Liu, P. Wang, Q. Zhao, H. Y. Yang, J. Wong, H. B. Sun, X. C. Dong, W. P. Lin and W. Huang, *Adv. Mater.*, 2012, **24**, 2901; (*c*) S. G. Hahm, N. G. Kang, W. Kwon, K. Kim, Y. K. Ko, S. Ahn, B. G. Kang, T. Chang, J. S. Lee and M. Ree, *Adv. Mater.*, 2012, **24**, 1062; (*d*) H. Zhuang, X. Xu, Y. Liu, Q. Zhou, X. Xu, H. Li, Q. Xu, N. Li, J. Lu and L. Wang, *J. Phys. Chem. C*, 2012, **116**, 25546; (*e*) Y. Liu, N. Li, X. Xia, J. Ge, Q. Xu and J. Lu, *Eur. Polym. J.*, 2011, **47**, 1160; (*f*) J. Liu, P. Gu, F. Zhou, Q. Xu, J. Lu, H. Li and L. Wang, *J. Mater. Chem. C*, 2013, **1**, 3947; (*g*) D. He, H. Zhuang, H. Zhuang, H. Liu, H. Liu, H. Li and J. Lu, *J. Mater. Chem. C*, 2013, **1**, 7883; (*h*) L. Shi, H. Ye, W. Liu, G. Tian, S. Qi and D. Wu, *J. Mater. Chem. C*, 2013, **1**, 7887.

10 (*a*) T. Kurosawa, Y. C. Lai, T. Higashihara, M. Ueda, C. L. Liu and W. C. Chen, *Macromolecules*, 2012, **45**, 4556; (*b*) F. Chen, G. Tian, L. Shi, S. Qi and D. Wu, *RSC Adv.*, 2012, **2**, 12879; (*c*) Y. Liu, Y. Zhang, Q. Lan, S. Liu, Z. Qin, L. Chen, C. Zhao, Z. Chi, J. Xu and J. Economy, *Chem. Mater.*, 2012, **24**, 1212; (*d*) S. G. Hahm, S. Choi, S. H. Hong, T. J. Lee, S. Park, D. M. Kim, W. S. Kwon, K. Kim, O. Kim and M. Ree, *Adv. Funct. Mater.*, 2008, **18**, 3276; (*e*) Q. Liu, K. Jiang, Y. Wen, J. Wang, J. Luo and Y. Song, *Appl. Phys. Lett.*, 2010, **97**, 253304–253311; (*f*) Y. Li, Y. Chu, R. Fang, S. Ding, Y. Wang, Y. Shen and A. Zheng, *Polymer*, 2012, **53**, 229; (*g*) G. Tian, S. Qi, F. Chen, L. Shi, W. Hu and D. Wu, *Appl. Phys. Lett.*, 2011, **98**, 203302; (*h*) L. Shi, H. Ye, W. Liu, G. Tian, S. Qi and D. Wu, *J. Mater. Chem. C*, 2013, **1**, 7387; (*i*) N. H. You, C. C. Chueh, C. L. Liu, M. Ueda and W. C. Chen, *Macromolecules*, 2009, **42**, 4456.

11 (*a*) D. B. Velusamy, S. K. Hwang, R. H. Kim, G. Song, S. H. Cho, I. Bae and C. J. Park, *Mater. Chem.*, 2012, **22**, 25183; (*b*) M. A. Khan, U. S. Bhansali, D. Cha and H. N. Alshareef, *Adv. Funct. Mater.*, 2013, **23**, 2145; (*c*) S. Gao, C. Song, C. Chen, F. Zeng and F. J. Pan, *J. Phys. Chem. C*, 2012, **116**, 17955; (*d*) C. J. Chen, Y. C. Hu and G. S. Liou, *Chem. Commun.*, 2013, **49**, 2804; (*e*) L. Q. Xu, B. Zhang, K. G. Neoh, E. T. Kang and G. D. Fu, *Macromol. Rapid Commun.*, 2013, **34**, 234; (*f*) M. A. Mamo, A. O. Sustaita, N. J. Coville and I. A. Hummelgen, *Org. Electron.*, 2013, **14**, 175.

12 (*a*) C. J. Chen, H. J. Yen, W. C. Chen and G. S. Liou, *J. Mater. Chem.*, 2012, **22**, 14085; (*b*) T. J. Lee, C. W. Chang, S. G. Hahm, K. Kim, S. Park, D. M. Kim, J. Kim, W. S. Kwon, G. S. Liou and M. Ree, *Nanotechnology*, 2009, **20**, 135204–135211; (*c*) K. Kim, H. J. Yen, Y. G. Ko, C. W. Chang, W. Kwon, G. S. Liou and M. Ree, *Polymer*, 2012, **53**, 4135; (*d*) Y. G. Ko, W. Kwon, H. J. Yen, C. W. Chang, D. M. Kim, K. Kim, S. G. Hahm, T. J. Lee, G. S. Liou and M. Ree, *Macromolecules*, 2012, **45**, 3749; (*e*) Y. L. Liu, K. L. Wang, G. S. Huang, C. X. Zhu, E. S. Tok, K. G. Neoh and E. T. Kang, *Chem. Mater.*, 2009, **21**, 3391; (*f*) T. J. Lee, Y. G. Ko, H. J. Yen, K. Kim, D. M. Kim, W. Kwon, S. G. Hahm, G. S. Liou and M. Ree, *Polym. Chem.*, 2012, **3**, 1276; (*g*) A. D. Yu, T. Kurosawa, Y. C. Lai, T. Higashihara, M. Ueda, C. L. Liu and W. C. Chen, *J. Mater. Chem.*, 2012, **22**, 20754; (*h*) H. J. Yen, C. J. Chen and G. S. Liou, *Adv. Funct. Mater.*, 2013, **23**, 5307.

13 (*a*) J. Ouyang, C. W. Chu, C. R. Szmanda, L. Ma and Y. Yang, *Nat. Mater.*, 2004, **3**, 918; (*b*) C. W. Chu, J. Ouyang, J. H. Tseng and Y. Yang, *Adv. Mater.*, 2005, **17**, 1440.

14 (*a*) F. Li, T. W. Kim, W. Dong and Y. H. Kim, *Appl. Phys. Lett.*, 2008, **92**, 011906; (*b*) F. Li, D. I. Son, S. M. Seo, H. M. Cha, H. J. Kim, B. J. Kim, J. H. Jung and T. W. Kim, *Appl. Phys. Lett.*, 2007, **91**, 122111.

15 J. S. Li, Y. J. Lin, H. P. Lu, L. Wang and S. P. Rwei, *Thin Solid Films*, 2006, **511**, 182.

16 (*a*) C. J. Chen, Y. C. Hu and G. S. Liou, *Chem. Commun.*, 2013, **49**, 2804; (*b*) A. D. Yu, C. L. Liu and W. C. Chen, *Chem. Commun.*, 2012, **48**, 383; (*c*) S. L. Lian, C. L. Liu and W. C. Chen, *Appl. Mater. Interfaces*, 2011, **3**, 4504; (*d*) Q. Zhang, J. Pan, X. Yi, L. Li and S. Shang, *Org. Electron.*, 2012, **13**, 1289; (*e*) J. C. Hsu, C. L. Liu, W. C. Chen, K. Sugiyama and A. Hirao, *Macromol. Rapid Commun.*, 2011, **32**, 528.

17 C. L. Tsai, C. J. Chen, P. H. Wang, J. J. Lin and G. S. Liou, *Polym. Chem.*, 2013, **4**, 4570.

18 (*a*) K. K. Ghuman and C. V. Singh, *J. Phys.: Condens. Matter*, 2013, **25**, 475501; (*b*) M. Rahman, D. MacElroy and D. P. Dowling, *J. Nanosci. Nanotechnol.*, 2011, **11**, 8642; (*c*) B. Ohtani, Y. Ogawa and S. I. Nishimoto, *J. Phys. Chem. B*, 1997, **101**, 3746.

19 (*a*) A. H. Yuwono, J. Xue, J. Wang, H. I. Elim, W. Ji, Y. Li and T. J. White, *J. Mater. Chem.*, 2003, **13**, 1475; (*b*) A. H. Yuwono, B. Liu, J. Xue, J. Wang, H. I. Elim, W. Ji, Y. Li and T. J. White, *J. Mater. Chem.*, 2004, **14**, 2978; (*c*) D. Eder and A. H. Windle, *J. Mater. Chem.*, 2008, **18**, 2036; (*d*) M. Miyauchi, *J. Mater. Chem.*, 2008, **18**, 1858; (*e*) A. Yu, G. Q. Lu, J. Drennan and I. R. Gentle, *Adv. Funct. Mater.*, 2007, **17**, 2600; (*f*) D. Fattakhova-Rohlfing, M. Wark, T. Brezesinski, B. M. Smarsly and J. Rathousky, *Adv. Funct. Mater.*, 2007, **17**, 123; (*g*) P. Tao, Y. Li, A. Rungta, A. Viswanath, J. Gao, B. C. Benicewicz, R. W. Siegel and L. S. Schadler, *J. Mater. Chem.*, 2011, **21**, 18623.

20 (*a*) H. W. Su and W. C. Chen, *J. Mater. Chem.*, 2008, **18**, 1139; (*b*) G. S. Liou, P. H. Lin, H. J. Yen, Y. Y. Yu, T. W. Tsai and W. C. Chen, *J. Mater. Chem.*, 2010, **20**, 531; (*c*) H. J. Yen, C. L. Tsai, P. H. Wang and G. S. Liou, *RSC Adv.*, 2013, **3**, 17048.

21 B. Cho, T. W. Kim, M. Choe, G. Wang, S. Song and T. Lee, *Org. Electron.*, 2009, **10**, 473.

